NASA TECHNICAL NOTE

NASA TN D-7096

NASA TN D-7096

ACOUSTIC PROPERTIES OF A SUPERSONIC FAN

by Arthur W. Goldstein, Frederick W. Glaser, and James W. Coats

Lewis Research Center
Cleveland, Ohio 44135

NATIONAL AERONAUTICS AND SPACE ADMINISTRATION • WASHINGTON, D. C. • JANUARY 1973

1. Report No.	2. Government Accession No.	3. Recipient's Catalog No.
NASA TN D-7096		

4. Title and Subtitle	5. Report Date
ACOUSTIC PROPERTIES OF A SUPERSONIC FAN	January 1973
	6. Performing Organization Code

7. Author(s)	8. Performing Organization Report No.
Arthur W. Goldstein, Frederick W. Glaser, and James W. Coats	E-6953
	10. Work Unit No. 501-24

9. Performing Organization Name and Address	11. Contract or Grant No.
Lewis Research Center National Aeronautics and Space Administration Cleveland, Ohio 44135	
	13. Type of Report and Period Covered
12. Sponsoring Agency Name and Address	Technical Note
National Aeronautics and Space Administration Washington, D.C. 20546	14. Sponsoring Agency Code

15. Supplementary Notes

16. Abstract

Tests of supersonic rotors designed to reduce forward propagating pressure waves and the accompanying blade passing tones and multiple pure tones showed the wave propagation and noise reduction to have been obtained at the expense of increased noise radiation rearward. Outlet guide vanes served to muffle the noise propagating rearwards, but did not affect forward propagation at all.

17. Key Words (Suggested by Author(s))		18. Distribution Statement
Noise	Rotating waves	Unclassified - unlimited
Transonic fan	Rotor shock waves	
Supersonic fan		

19. Security Classif. (of this report)	20. Security Classif. (of this page)	21. No. of Pages	22. Price*
Unclassified	Unclassified	38	$3.00

* For sale by the National Technical Information Service, Springfield, Virginia 22151

ACOUSTIC PROPERTIES OF A SUPERSONIC FAN

by Arthur W. Goldstein, Frederick W. Glaser, and James W. Coats

Lewis Research Center

SUMMARY

Three supersonic fan rotors and one complete stage were tested for acoustic properties. They were designed to reduce forward radiation of blade passing tones by eliminating shock waves and expansion waves propagating forward. The designs incorporated large blade-to-blade spacing to eliminate flow choking in the outer blade channels and also incorporated flat suction surfaces to eliminate other waves attached to the blades.

The main pressure wave system was eliminated from the front of the rotor as the blade design was expected to do, and the gains were reflected as reduction of far-field sound in front of the rotors and fan at supersonic speeds. At subsonic conditions the complete stage produced more noise rearwards than the rotor alone because of rotor blade wakes interacting with the stator vanes. At supersonic conditions, the noise propagating rearwards was reduced because the presence of stator vanes damped out the pressure waves rotating with the rotor. Forward noise propagation was not affected by the presence of the stator vanes.

The residual noise then remaining was much smaller than the noise originating from the leading-edge bluntness of the blades. A more elaborate model is needed to explain the level of this noise.

INTRODUCTION

The fan component of high-bypass turbofan engines is a principle source of noise. Both the broadband noise and discrete-tone noise generated by the fan are reduced by designing the fan to operate at low (subsonic) rotor speed; additionally, low-rotor speed results in reduced transmission of the rotor tones and also of the rotor-stator interaction tones from the fan through the ducting to the exterior. Additional reduction in external noise radiation can also be achieved by treating the inside of the nacelle with sound absorbing material. Unfortunately, the low-speed fans require the use of a low-speed turbine of many stages and a larger weight compared with a high-speed turbine

delivering the same power. In deciding whether to use a high-speed or low-speed fan when designing an engine, overall system considerations then involve a trade-off between the weights of the turbine and of the sound absorption materials employed in the fan nacelle. The present investigation is aimed at the reduction of the noise output of a transonic fan that will permit a reduction of the total amount of sound absorbing materials required, thereby improving the efficiency of the propulsion system when designed to operate under a noise limitation constraint.

Noise output of transonic fans consists of incoherent (or broadband) noise, discrete tones at the blade-passing frequency (and overtones), and a series of discrete tones which have frequencies that are multiples of the rotor rotational frequency (also called multiple pure tones). In transonic fans the broadband noise is a small part of the acoustic output; it is not considered further here.

The blade-passing tone often originates from the interaction of the wakes of the rotor blades with the stator vanes or from the rotating shock and expansion waves that arise in the supersonic flow relative to the rotor blades and that are fixed relative to those blades. (Pressure disturbances originating in subsonic relative flow do not produce a flow of acoustic energy and are rapidly damped out. Data presented in this report will confirm this distinction between disturbances to subsonic flow and to supersonic flow.) The transonic rotor produces three types of these shock - expansion-wave configurations.

One type has a normal shock wave standing ahead of each blade leading edge and channel entrance, extending upstream of the rotor. (See fig. 1 and refs. 1 and 2.) If the rotor is designed to swallow this normal shock at the channel entrance, a potent source of noise is eliminated.

A second type of wave system can arise when the detached shock system is swallowed (fig. 2). This occurs when the operating Mach number is sufficiently high. In this case a curved suction surface of the blading initiates expansion waves that progress upstream (with subsonic axial velocity component) with a balancing shock wave attached to the leading edge of the blade. The noise produced by this wave system was estimated for a rotor operating at

Relative Mach number	1.6
Flow angle to axis, deg	70
Supersonic turning, deg	10
Number of blades	40
Axial distance upstream, fraction of tip diameter	1/2
Noise sound pressure level, dB	158

The method of Fink (ref. 3) was used in this estimate. It is this noise that the experi-

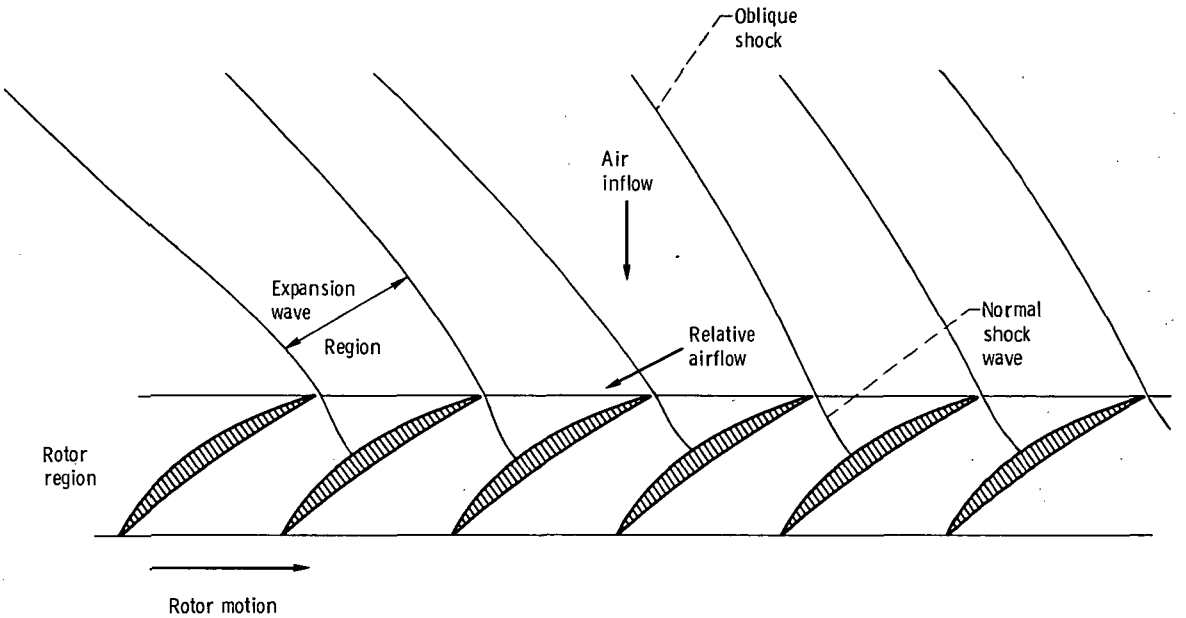

Figure 1. - Blading with detached shock waves.

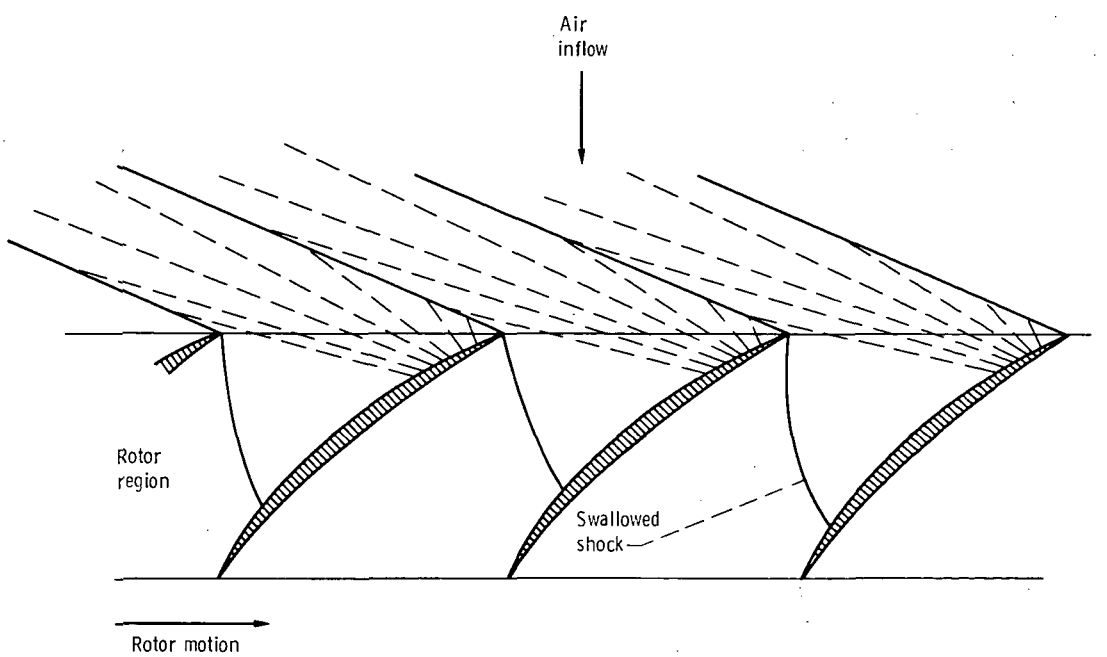

Figure 2. - Blading with attached shock waves.

mental blades discussed herein are designed to reduce, by eliminating the corresponding wave system.

The blades were also designed to eliminate the noise that arises from detached shock waves, which rotate with the blades. This third wave system arises from the nonzero thickness of the leading edges of the blades.

The tests reported herein had the objectives of determining the noise levels of the rotor at Mach numbers below and above that required for establishing or starting the design wave-configuration, determining if the expected decrease in front-propagating noise level was achieved, and determining the nature of the residual noise. Deflection of the waves rearward would increase the noise propagation there, but the sound-absorbing treatment, which would be used in the rear to absorb the sound originating on the rear-facing surfaces of the blades, would also absorb the waves reflected rearward. Partially completed work was reported in reference 4.

FAN AERODYNAMICS

Wave System

The blades designed to eliminate both the detached shock waves and also the attached wave system with the accompanying blade-passing-tone noise and multiple pure tones are made according to the following principles. The blade chords (fig. 3, blade design 1) are made sufficiently short relative to the blade spacing to, in effect, eliminate the channel or passageway between adjacent blades; the blades are, therefore, like a set of isolated bodies in that a channel area limitation cannot be the cause of a detached shock (as in

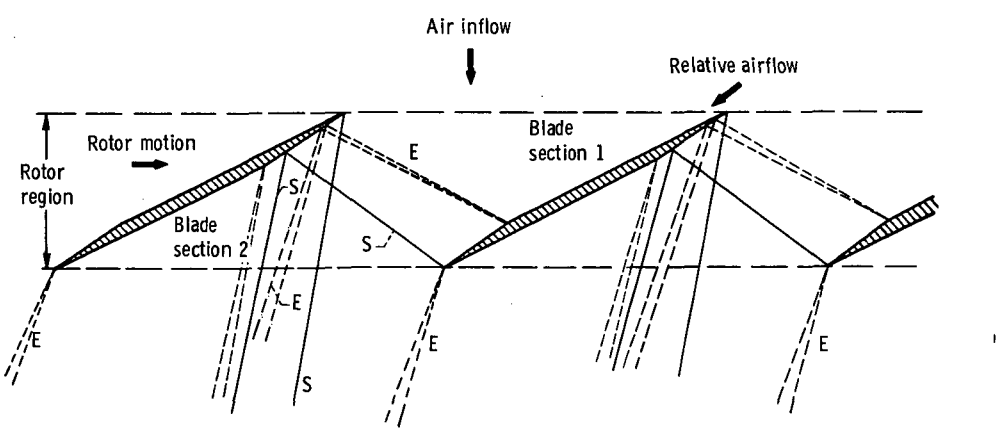

Figure 3. - Supersonic rotor blade sections - minimal upstream disturbance; blade design 1. (S denotes shock waves; E expansion waves.)

fig. 1). The attached shock and suction-surface expansion wave (fig. 2) are eliminated by using a straight suction surface for the blade in the region that could give rise to waves traveling upstream.

Any pressure wave originating on the suction surface is intercepted by the following blade and reflected downstream (fig. 3). When such waves traveling upstream from the blade surface are eliminated, the air inflow direction is parallel to the exposed portion of trailing surface; the bow wave, which results from the angle of incidence and extends upstream of the rotor, is also eliminated. The gas is therefore deflected through the wedge angle on the pressure surface of the blade by a downstream-progressing shock wave. This wave is part of a system of waves (fig. 3) that are generated by the blade thickness. The wave system generated by blade thickness is shown more clearly in figure 4 (blade design 2).

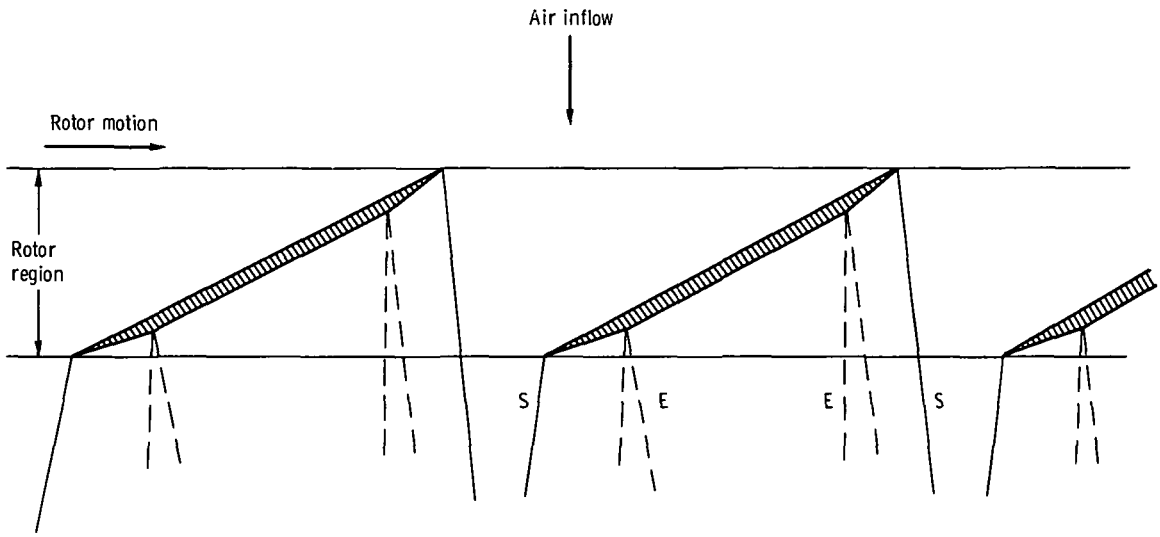

Figure 4. - Waves caused by blade thickness alone; blade design 2. (S denotes shock waves; E expansion waves.)

A downstream system of waves is associated with the blade loading and compression of the gas. The blades are loaded by throttling the fan exhaust, thereby causing a wave pair to originate on the blade trailing edge; a compression wave travels upstream from the trailing edge and reflects on the pressure surface of the following blade, while the expansion wave travels downstream (see fig. 5). The reflected shock generates a high pressure on the pressure surface of the following blade and thereby produces the torque force required for shaft work.

The establishment of the wave system (thickness and loading effects), depends on the approach Mach number being sufficiently high so that deflection of the gas through the leading-edge wedge angle can be accomplished by an attached wave.

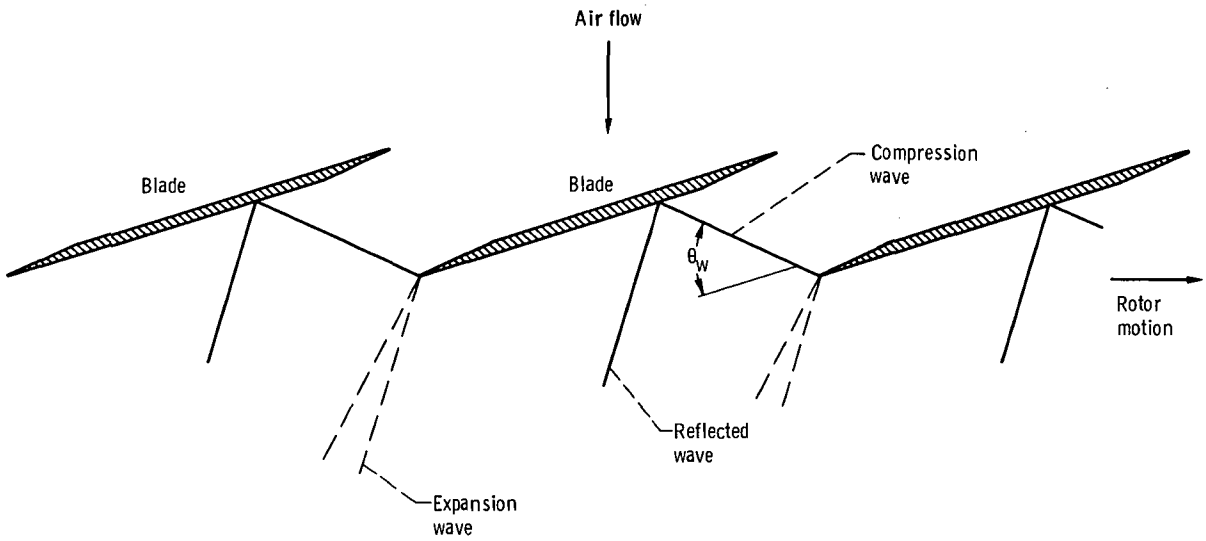

Figure 5. - Waves caused by moderate blade loading; blade 1.

There are residual waves propagating forward in addition to the waves already described. The third type of wave system that propagates upstream arises from the nonzero-thickness of the leading edges of the blades (fig. 6). There is a detached shock wave followed very closely by a family of expansion waves; this wave group interacts mutually to decrease amplitude with distance from the rotor face (refs. 3 and 5). The amplitude of noise produced by this wave system was estimated by the method of references 2 and 5 to be about 151 decibels for the conditions of the previous estimate and with leading-edge thickness assumed to be 0.007 times the blade spacing. In this particular case the estimated total blade passing noise of 159 decibels would be reduced 8 decibels by eliminating the suction surface waves.

One residual noise is the multiple pure tone sequence, the frequencies of which are integral multiples of the rotor frequency rather than of the blade passing tone. These have been reported in references 6 to 10. Additional detailed analyses of this noise have been presented in references 3, 11, and 12. These analyses are based on the model proposed in reference 6 in which there is a shock and expansion wave system initiated from each blade. As upstream distance from the rotor increases, the shocks and expansion waves interact and decrease in strength; with this, the intensity of the blade passing tone decreases. However, the variation of wave amplitude from one wave to the next does not decrease as rapidly, so that, with some initial irregularity of shock waves, the spatial distribution becomes more and more irregular with increasing upstream distance from the rotor. This evolution manifests itself in the spectrum by an increasing proportion of tones that are multiples of the rotor frequency, since the pattern tends more to repetition with a complete rotation rather than from blade to blade.

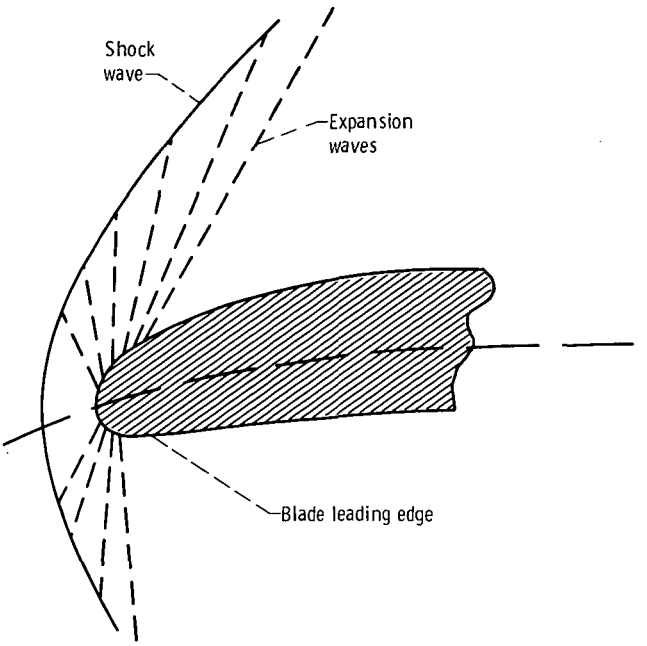

Figure 6. - Waves caused by nonzero thickness of leading edges.

In addition to the calculations of references 3, 11, and 12, data presented in reference 10 confirm the theory. This theory implies that the multiple pure tones could be reduced simultaneously with the upstream-propagating waves and the blade passing tone.

Another residual wave configuration is essentially three dimensional. If there is a spanwise variation of incidence angle, expansion waves can originate from one section of the blade span, and compression waves from another. These waves could arise from built-in twist or from boundary layers on the inner and outer casing; the portion of the blades projecting into the boundary layer would originate expansion waves, and the remainder would originate compensating compression waves.

Pressure Ratio

The aerodynamic loading capability of the blade can be translated into the capability of increasing the pressure of the pumped air. If only the trailing-edge waves are considered and blade thickness and camber are neglected, the trailing edge shock wave with wave angle θ_w (fig. 5) to the gas flow direction will impinge on the following blade at a point from which the distance along the blade to the trailing edge is C_a (for a complete list of symbols see appendix A). This portion of the thin, uncambered blade is the only section that is loaded. Let the pressure rise produced by the wave be Δp and the

pitch angle (chord line to fan rotation axis) be α. Then

$$C_a = - S \frac{\cos (\theta_w + \alpha)}{\sin \theta_w}$$

where S is the tangential spacing of the blading. The tangential force is

$$F_\theta = C_a \Delta p \cos \alpha$$

and the rate of work per blade on the gas (per unit of blade span) is UF_t, where U is the rotational speed of the blades. The mass flow through one blade interspace per unit of span upstream of the shock is $\rho V_z S$, where ρ is the gas density and V_z is the axial component of gas velocity. Then the work input per unit mass, equal to the rise in stagnation enthalpy, is

$$\Delta H_T = UC_a \Delta p \frac{\cos \alpha}{\rho V_z S}$$

From this, the stagnation temperature rise ratio is

$$\frac{\Delta T_T}{T_T} = \left(\frac{\gamma - 1}{\gamma}\right)\left(\frac{\Delta p}{p}\right)\frac{C_a}{S} \cos \alpha \frac{\tan \alpha}{1 + \frac{\gamma - 1}{2}\left(M_z^2\right)}$$

where M_z is the Mach number, γ is the ratio of specific heats, and p is the stream pressure upstream of the shock. To find out what aerodynamic loading capability could be expected for the blade, the following calculation was made. For an assumed relative Mach number of 1.6, $M_z = 0.6$, adiabatic efficiency of 85 percent, and pressure rise $\Delta p/p$ corresponds to a Mach number of 1.0 after a reflected shock wave, the calculated pressure ratio is 1.65. This is certainly a pressure ratio suitable for some propulsion applications. The experimental study reported herein was not designed to attain these values, but to demonstrate a novel way to minimize upstream wave propagation.

TEST EQUIPMENT AND PROCEDURE

Fan Test Rig

The fan test rig is designed with a cantilevered rotor so that no supports project through the internal air stream. An overall view of the fan installation is shown in figure 7 and additional details are displayed in figure 8. The front fairing, the outside

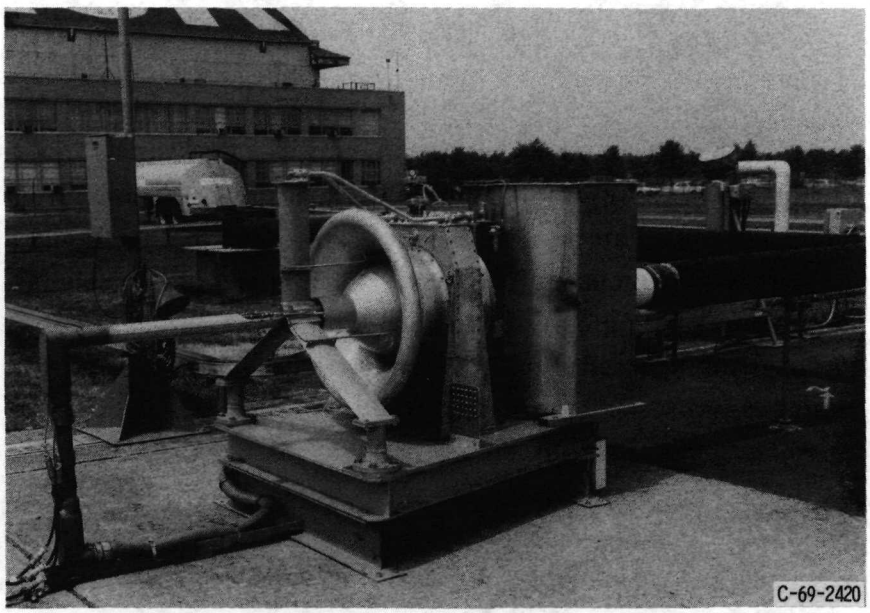

Figure 7. - Supersonic fan test rig.

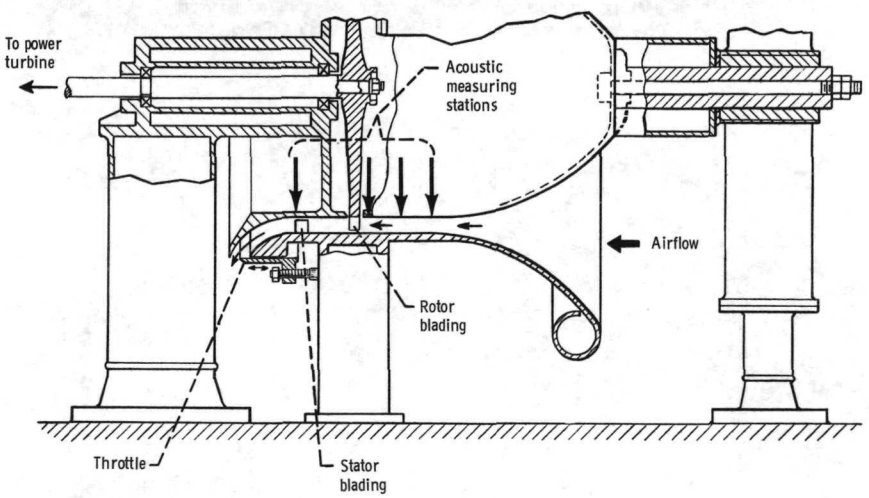

Figure 8. - Blade test with unobstructed flow path.

casing, and the combination of rotor bearings and internal casing are all supported independently by the test bed. The exhaust throttle is a sliding circular cylinder that provides circumferentially symmetrical throttling. The fan was driven by an air turbine using the laboratory air supply.

Details of the blade shape are shown in figure 9. Blade design 1 was tested first

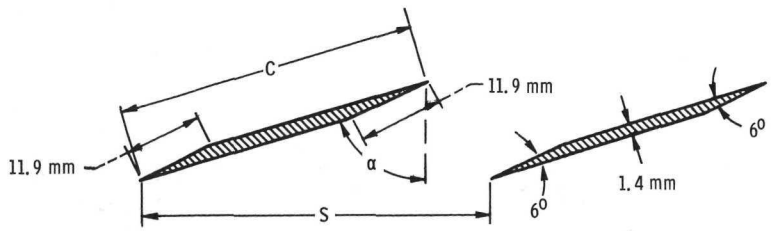

Blade design 1

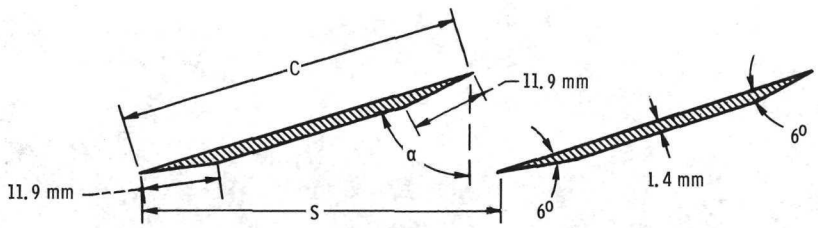

Blade design 2

Blade design	S				α, deg		C		Relative gas Mach number	
	Root		Tip		Root	Tip	mm	in.		
	mm	in.	mm	in.						
1	49.10	1.934	55.22	2.175	73	{73 / 75}	46.8	1.84	1.33	1.48
2	49.10	1.934	55.22	2.175	72	74	49.1	1.93	1.33	1.48

(a) Rotor blade design parameters. Tip diameter, 45.75 centimeters (18 in.); hub diameter, 40.64 centimeters (16 in.); rotor speed, 20 000 rpm; number of blades, 26; rotor blade difference factor, 0.10; rotor tip speed, 480 meters per second (1574 ft/sec).

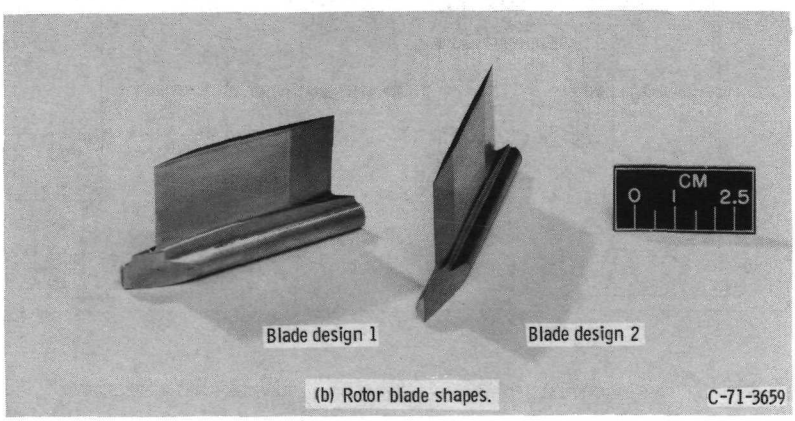

Figure 9. - Rotor blade dimensions and shape.

with all sections the same (untwisted or prismatic shape). It was also tested after being twisted so as to provide uniform incidence. Blade design 2 was designed to avoid all waves propagating upstream from the suction surface and was twisted for constant incidence angle. All blades were ground to shape and formed with the root attachment from a single piece of metal. The blades were slid into broached wheel slots, and no significant differences existed in blade shape, blade location, or blade orientation, from one to the next; the rotor may be regarded as having exactly periodic blading. The details of the stator blade design are shown in figure 10.

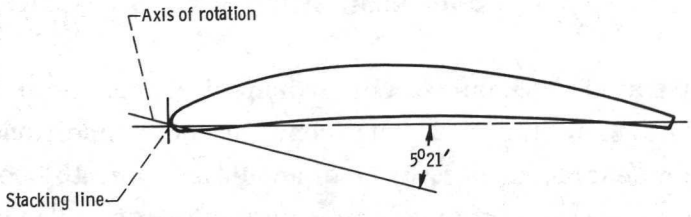

(a) Typical stator airfoil.

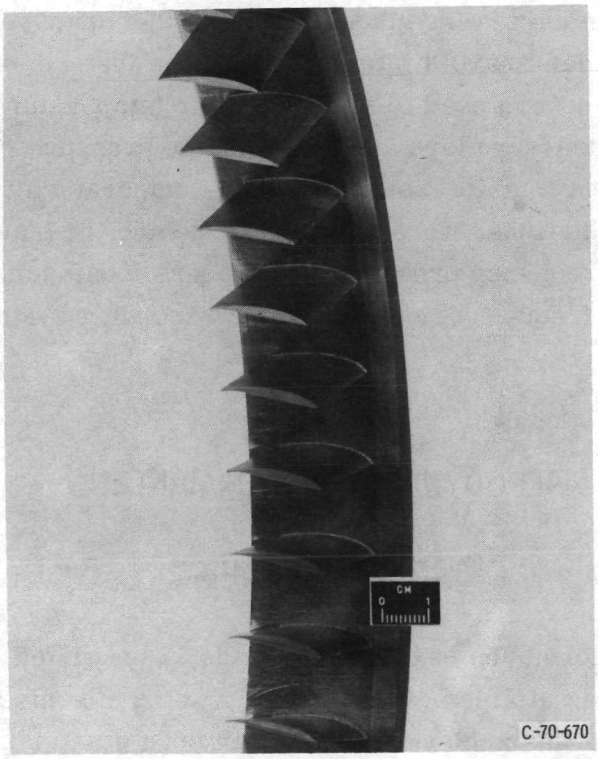

(b) Stator ring assembly.

Figure 10. - Stator blade deisgn. Series 65 airfoil; circular arc meanline; 10 percent thick; stator chord, 23.2 millimeters (0.918 in.); number stator blades, 69; no twist, hub to tip.

In front of the rotor was an annular cylindrical duct containing acoustic measuring stations located at the following distances upstream of the rotor leading edge: 1.07, 6.04, and 11.12 centimeters (0.42, 2.38, and 4.38 in.). There was an additional station located at the stator discharge 8.92 centimeters (3.51 in.) behind the rotor blade trailing edges. The front cylindrical section was blended into a bellmouthed intake 11.12 centimeters (4.38 in.) upstream of the rotor face (fig. 7).

Data Acquisition

The fan rig was operated in an outdoor environment. Acoustic measurements in the far field were made 3.81 meters (12.5 ft) from the rotor; additional internal measuring stations have been described. Analysis of acoustic data into one-third octave band pass spectra was done on line and from magnetic tape records. The analyzer used on line had an approximate time constant of 3 seconds. When the data recorded on magnetic tape were used, the analyzer employed permitted 32-second samples to be analyzed.

Aerodynamic measurements were made at a time other than when acoustic measurements were made in order to avoid interference of the instrumentation with the fan noise. Nine thermocouples were used to survey the air temperature just inside the bellmouth. Three static-pressure taps and atmospheric pressure provided the mass flow data. Two downstream total-pressure and total-temperature rakes, each providing five radial measuring stations, were located just behind the stator. Additional data were obtained from high-frequency pressure transducers located upstream and downstream of the rotor. The frequency response of the recording system ranged from 3 hertz to 20 kilohertz.

AERODYNAMIC PERFORMANCE

Overall Performance

The aerodynamic performance of the stage (blade 1, untwisted) is shown in figure 11. The expected mass flow was attained. Consequently we have some assurance that the desired wave configuration was achieved at the mean span position. The efficiencies obtained at high speed are too low for direct use of this design, and two possible reasons are presented. First, the blades could not be loaded adequately by closing down the back throttle because of the limited power available from the drive turbine at 70 percent of design speed and higher. The diffusion factor of the blading was only 0.1,

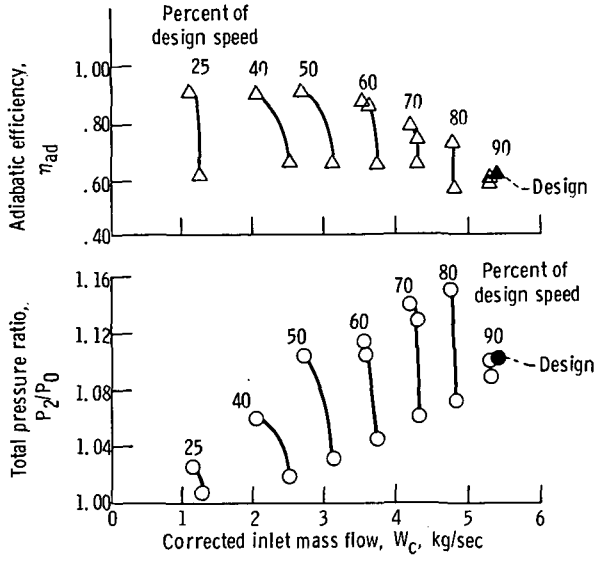

Figure 11. - Stage aerodynamic performance; blade 1, untwisted.

whereas values of 0.5 to 0.6 are often used in practice. As a result, energy losses occur in the fan that are a large percentage of the energy input to the gas, and the efficiency is low. Secondly, the blades were designed with a short span to approximate a two-dimensional flow. The short span of the blades results in relatively important end losses, which are generally much higher than midspan losses.

Rotor Pressure Field

The variation of pressure with time at a close upstream location (1 cm from the rotor face) was expected to give an indication of the wave system. A series of oscilloscope traces of these data are shown in figure 12. These were obtained with blade shape 1, untwisted. As the rotor speed increases from low supersonic speed (15 000 rpm) to high supersonic speeds (18 000 and 19 400 rpm), the pressure amplitude falls off. Although these data are not suitable for detailed amplitude calculation because of the extreme and unexpected variability of the pressure and flow from one blade space to the next, some characteristics can be noted. Two traces obtained at different azimuthal stations during rotor operation at 15 000 rpm, indicate pressure fluctuations as much as 1723 newtons per square meter (0.25 psi). At this speed the rotor is operating in barely supersonic flow, and pressure waves should be propagating forward. Especially noteworthy is the irregularity of the waves at one of the measuring stations (fig. 12(b)). Such irregularities are the obvious cause for multiple pure tones, which

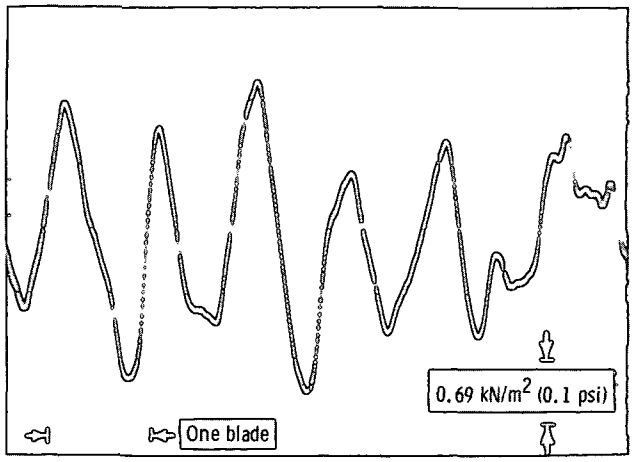

(a) Rotor speed, 15 000 rpm; azimuthal station 1.

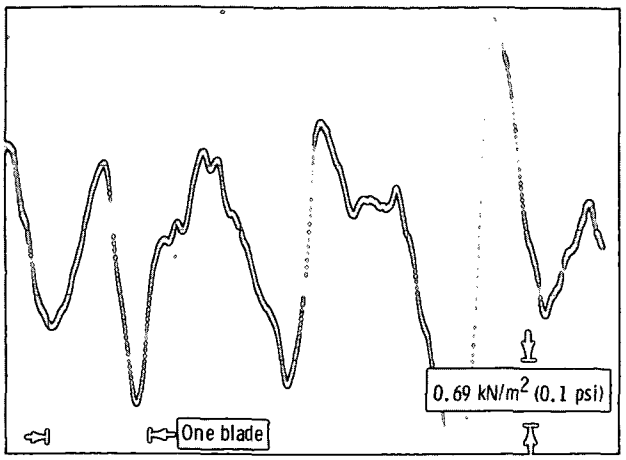

(b) Rotor speed, 15 000 rpm; azimuthal station 2.

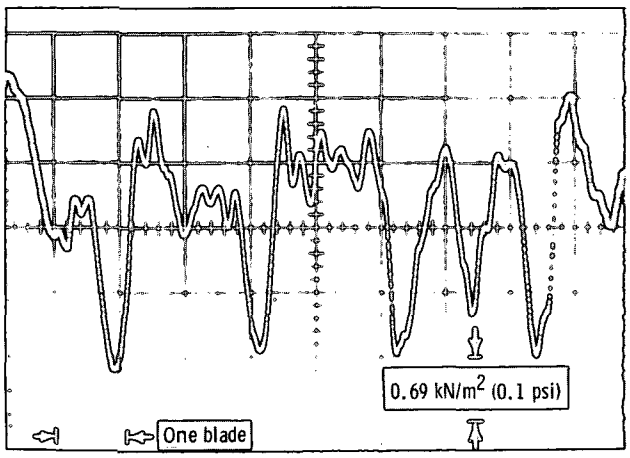

(c) Rotor speed, 18 000 rpm.

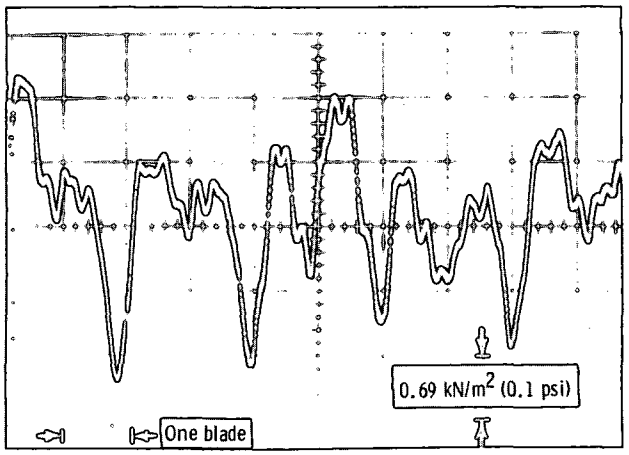

(d) Rotor speed, 19 400 rpm.

Figure 12. - Pressure - time history at rotor face. Blade 1, untwisted; distance upstream of rotor, 1.1 centimeters (0.42 in.).

show up in the spectrum of the noise. At 18 000 rpm the calculations indicate that the transfer of the waves from the front to the back should be occurring; the pressure trace shows that this process proceeds more completely for some blades than others.

The same effect is shown when the blade is twisted to reduce spanwise incidence variation (see fig. 13). The process of transfer of the waves from the front to the rear of the blade, as the gas approach speed is increased from low supersonic to higher supersonic speed with increased rotor speed, can be visualized as follows. At low supersonic flow velocity, the expansion wave proceeds upstream from the suction-surface deflection location in a wave that approaches, from the perpendicular direction, the relative flow vector. The wave, therefore, passes entirely ahead of the following blade and upstream of the rotor. In the present case this wave provides a 6° expansion deviation and increases the Mach number of the flow striking the following blade leading

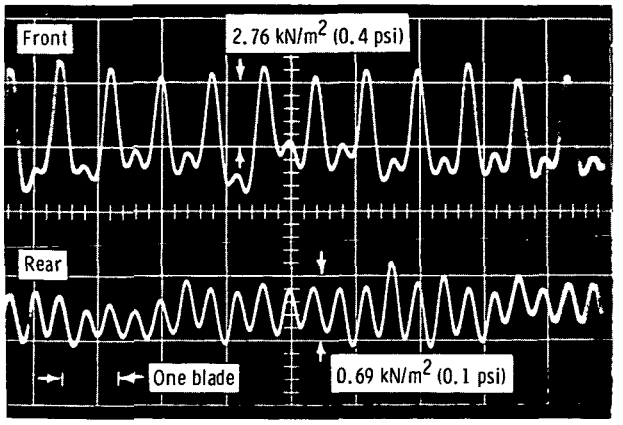

(a) Rotor speed, 14 300 rpm.

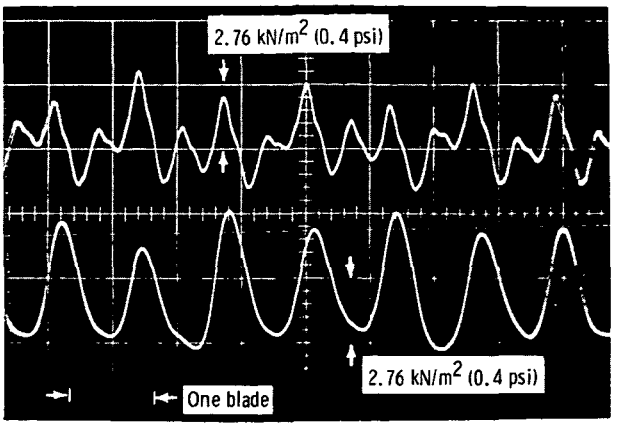

(b) Rotor speed, 17 300 rpm.

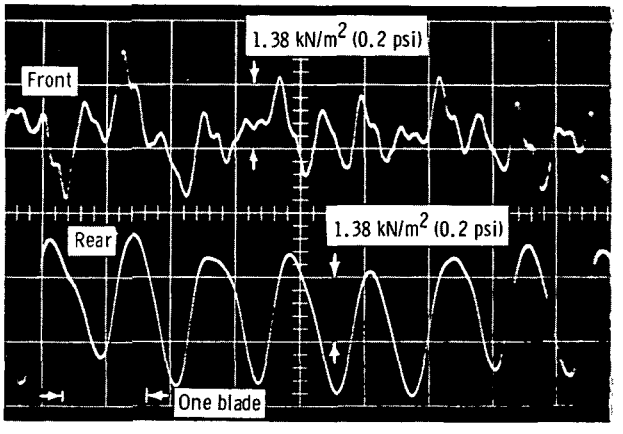

(c) Rotor speed, 18 300 rpm.

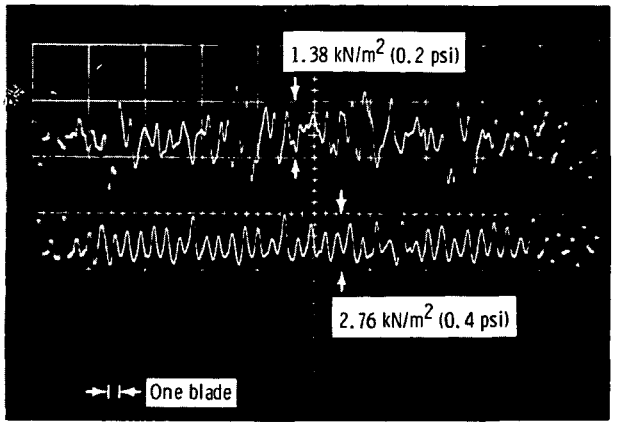

(d) Rotor speed, 19 200 rpm.

Figure 13. - Pressure - time history at rotor face; blade 1, twisted. Distance upstream of rotor: front traces, 1.1 centimeters (0.42 in.); rear traces, 8.9 centimeters (3.51 in.).

edge to a level such that a full 6° deflection shock wave could be attached to the blade leading edge. (Relative sonic approach speed at the blade tip is estimated to have occurred at 13 700 rpm and at the blade roots at 15 200 rpm.) The expansion wave occupies a finite width, and, as the operating speed of the rotor is increased and its direction changes closer to the flow direction, part of the wave is caught and reflected downstream by the next blade (see fig. 24). The expansion wave in front of the rotor is thereby decreased from a 6° deflection to less. As a general principle, the expansion waves proceeding upstream must be exactly matched by the compression shocks in order to establish a zero axial acceleration along the annulus inlet to the rotor. Thus, the deflection shocks attached to the leading edges of the blades must also weaken as the expansion waves are increasingly reflected with speed. The remainder of the deflection of the flow around the 6° wedge angle of the blade must, therefore, be accomplished on the downstream-facing side of the blade. Reflection is estimated to begin

at 14 300 rpm at the blade tips and at 15 200 rpm at the blade roots. When the velocity is sufficiently high, all the expansion wave is reflected downstream, and the upstream branch of the bow shock of 6° is eliminated (see fig. 3). This condition is estimated to be achieved at 19 300 rpm at the blade roots and 19 700 rpm at the blade tips. At 19 400 rpm (fig. 12) the trace shows a blade passing tone, although it was expected that this would not be present if the bow wave were transferred from the front of the cascade to the rear, as planned. The fact that a substantial level of pressure fluctuation persists may be related to the lack of twist of these blades or to the bluntness of their leading edges.

The effect of twist may be estimated as follows: At 18 000 rpm and at the mean radius of 21.62 centimeter (8.515 in.), the rotor speed is 320 meters per second (1260 ft/sec). Since the blade stagger angle is 73°, the axial velocity is 104.5 meters per second (412 ft/sec). With this value for axial velocity, the rotor-speed at the tip results in a relative gas flow angle of 73° 46' and at the hub of 72°. The blade angle is the same at all locations, and the resultant angle of attack is -1° at the hub and 0.75° at the tip. As previously stated, these values may be influenced by the tip or hub operating in the boundary layer. This would cause spanwise variation of incidence angle. Expansion waves can then originate from one section of the blade span, and compression waves from another. At the hub the Mach number is 1.205, and the compression wave radiating from the leading edge causes a rise in pressure of 5.3 percent, or 4.9 kilonewtons per square meter (0.71 psi). At the blade tips the pressure drop in the expansion wave is 3.93 kilonewtons per square meter (0.57 psi). The size of the opening to the instruments and the limitations of the amplifying system do not permit a sharp waveform to be exhibited, so one can expect only the first few harmonics of the wave to show. The fundamentals of the saw-toothed waves of these amplitudes would be 3.12 kilonewtons per square meter (0.45 psi) at the hub and 2.5 kilonewtons per square meter (0.36 psi) at the tip. There will be a further reduction in amplitude because of interaction of the waves from the blade roots and tips. The observed pressures were about 1.38 kilonewtons per square meter (0.2 psi), on the average, so that this mechanism provides a plausible explanation of the pressures observed.

ACOUSTIC PERFORMANCE

Sound Spectrum Produced

Spectrograms of the noise produced by the rotor and measured at the station 1 centimeter upstream are displayed in figure 14 (rotor with blade 1, untwisted). The spectrum at low speed (10 000 rpm) has a blade passing tone and a series of discrete

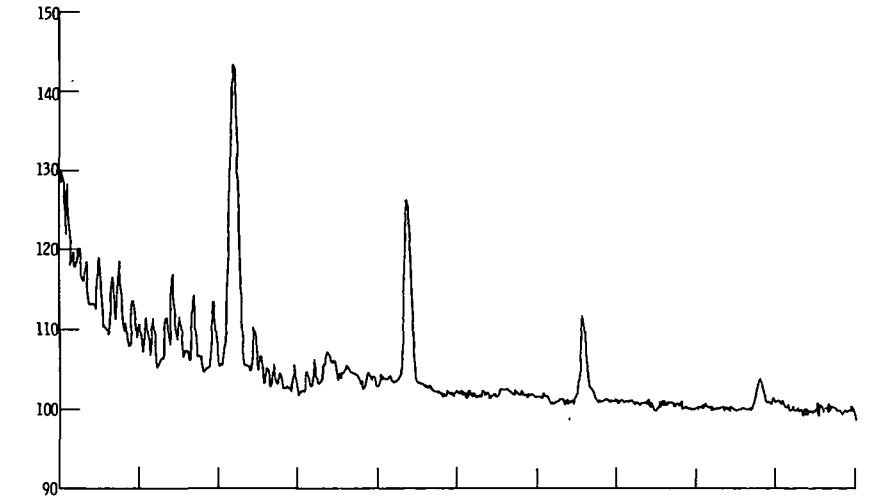

(a) Rotor speed, 10 000 rpm.

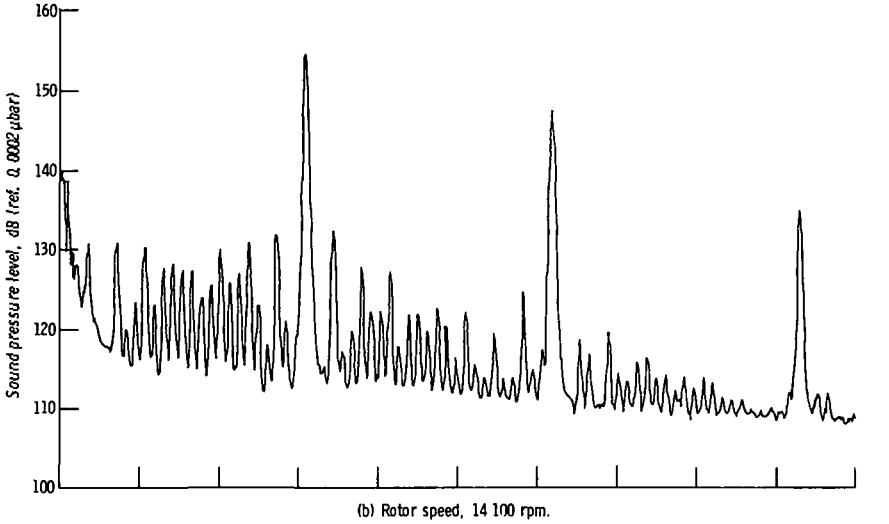

(b) Rotor speed, 14 100 rpm.

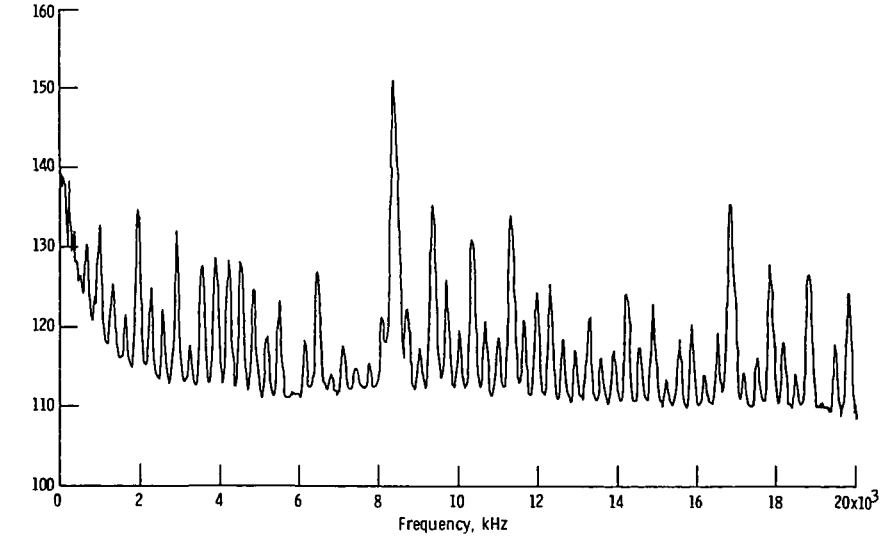

(c) Rotor speed, 19 300 rpm.

Figure 14. - Spectrogram at face of rotor with blade 1, untwisted. Distance upstream of rotor, 1.1 centimeter (0.42 in.).

tones, all harmonics of the shaft speed. These tones have been previously reported as having been observed only at supersonic flow conditions (refs. 6, 7, and 9). Mather, Savidge, and Fisher have observed such tones in the far acoustic field of a rotor turning at subsonic speeds (fig. 4(a) of ref. 8). (Their paper is not clear on whether the rotor had sufficient housing to dampen these rotor tones.) The presence of the tones at low speed indicates that they result from azimuthal pressure distributions, which are not identical from one blade space to the next. These nonperiodic pressure distributions were demonstrated in the pressure-time traces of figure 12. At 14 100 rpm (fig. 14) the outer annulus of the rotor is operating at supersonic speed; the spectrogram for this case shows a higher level of the rotor harmonic tones. The nonuniformities of the blading were not the cause of the nonperiodicity of the pressure distribution. These blades were machined and ground to extremely close tolerances and fitted into broached slots in the wheel. Therefore, the observed nonperiodicity of the pressure is believed to be a result of instability of the exactly periodic flow distribution.

The variation of pressure from one blade channel to the next does increase somewhat relative to the blade pressure waves as the speed is increased, but the blade passing waves are always dominant. The spectrograms shows that at 14 100 rpm the blade passage fundamental is 22 decibels higher than the largest of the rotor harmonics. At all other supersonic speeds the spectrograms were also dominated by the blade passing tone, which is generated by a propagating shock wave at or above speeds of 14 000 rpm. Similar spectra are seen in the sound generation for blades 1 twisted, and 2 (figs. 15 and 16).

Acoustic Amplitudes

The amplitude of the wave generation varies with speed as indicated by the plot in figures 17 to 19 (OASPL against rotor speed). The first set of blades (figs. 17 and 18) produces an increase with speed, a decrease just after the velocity approaching the blades becomes sonic over the entire span, and then a rise. As previously explained in connection with the pressure charts, the forward propagating wave system begins to weaken between 14 300 and 15 200 rpm. The sound measured should therefore show a decrease beginning there and continuing to 19 700 rpm, at which speed the transfer of the wave system from the front to the back is completed. Simultaneously with the decrease in noise propagating forward, the expansion wave is being reflected rearwards, which produces more noise propagating rearwards. Figures 20 and 21 show this to be the case. The noise ahead of the rotor reaches a maximum at 15 000 rpm and falls off as speed increases, whereas the noise behind the rotor continues to increase as the speed increases, and levels off at a much higher intensity than the noise in the front of

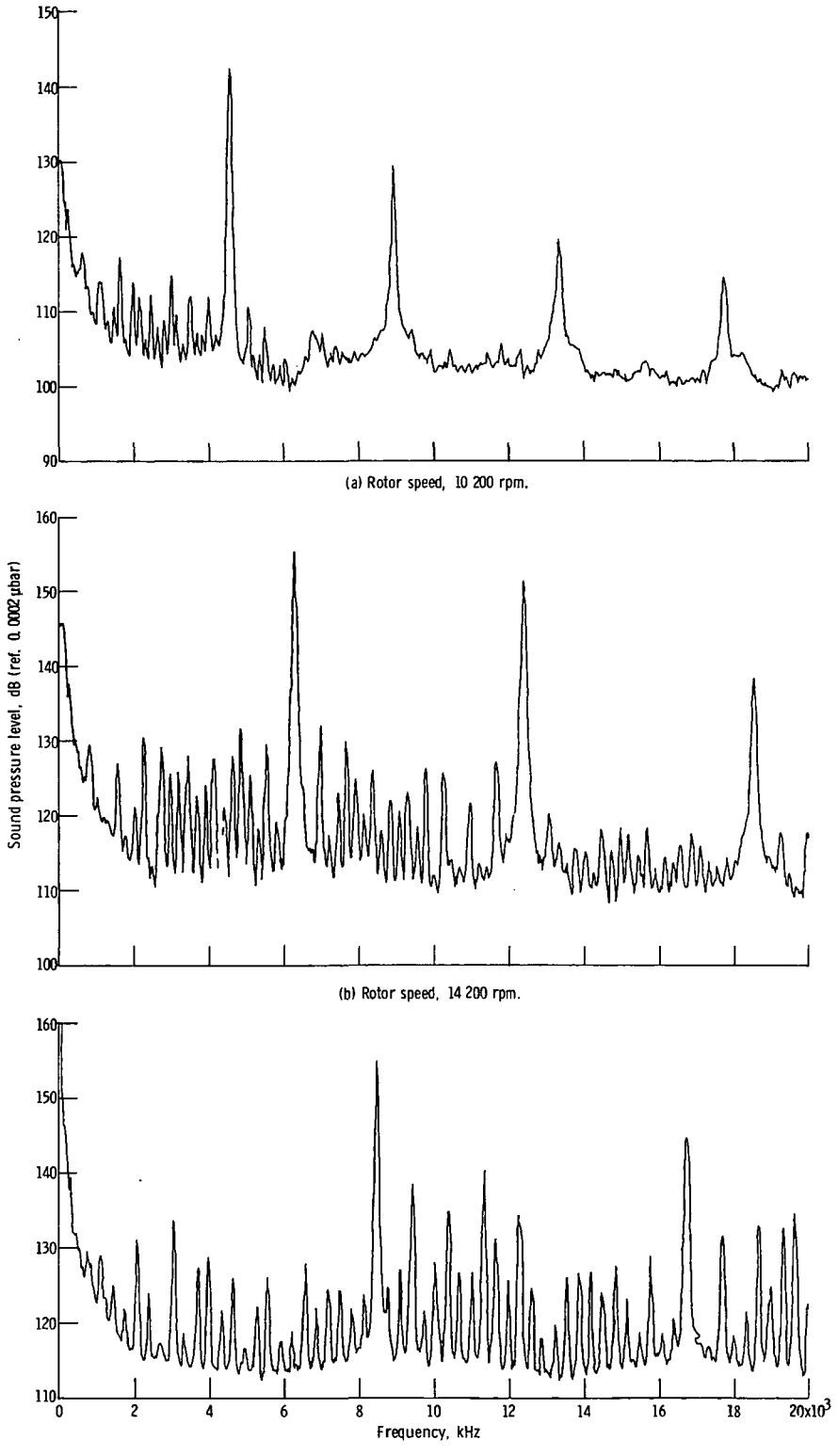

Figure 15. - Spectrogram at face of rotor with blade 1, twisted. Distance upstream of rotor, 1.1 centimeter (0.42 in.).

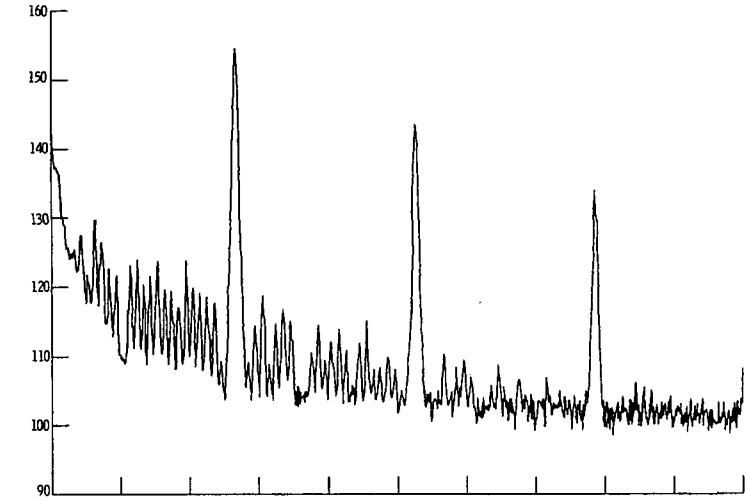

(a) Rotor speed, 12 000 rpm.

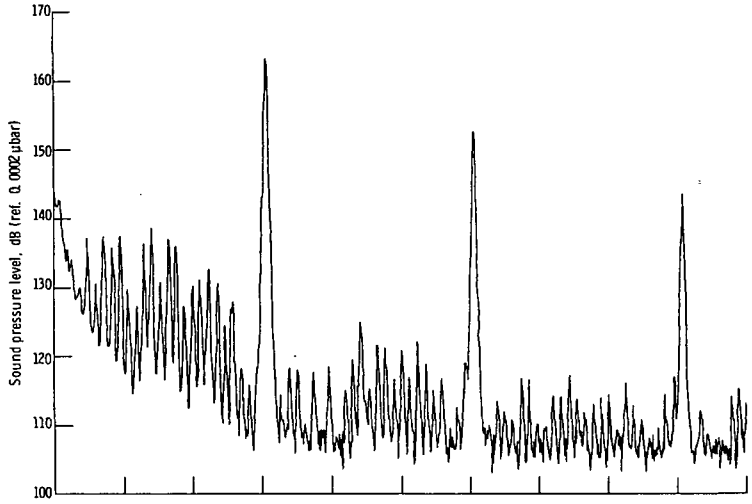

(b) Rotor speed, 14 000 rpm.

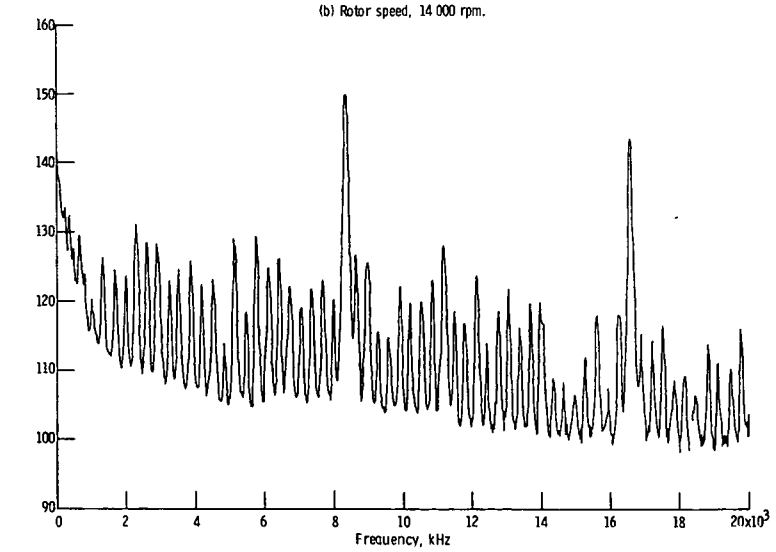

(c) Rotor speed, 19 200 rpm.

Figure 16. - Spectrogram at face of rotor with blade 2. Distance upstream of rotor, 1.1 centimeter (0.42 in.).

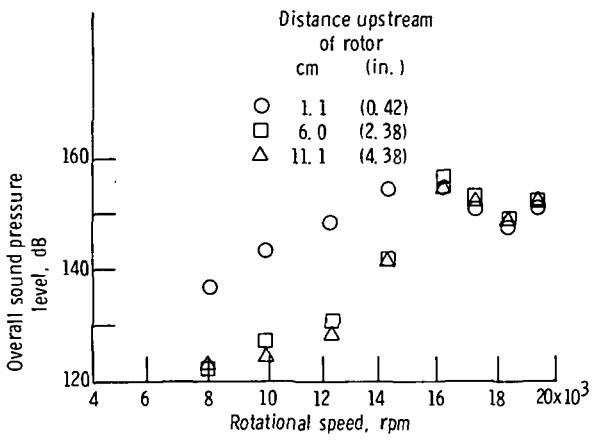

Figure 17. - Overall sound pressure level upstream of rotor with blade 1. Untwisted blades; rotor alone.

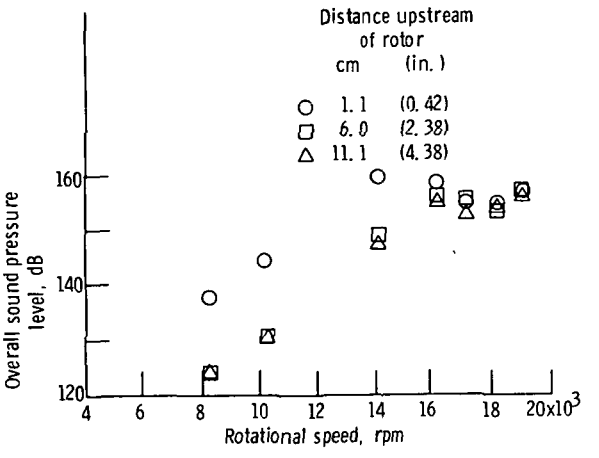

Figure 18. - Overall sound pressure level upstream of rotor with blade 1. Twisted blades; rotor alone.

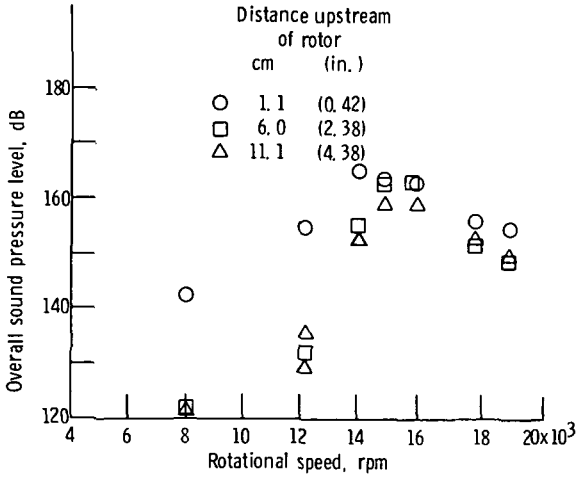

Figure 19. - Overall sound pressure level, upstream of rotor with blade 2. Rotor alone.

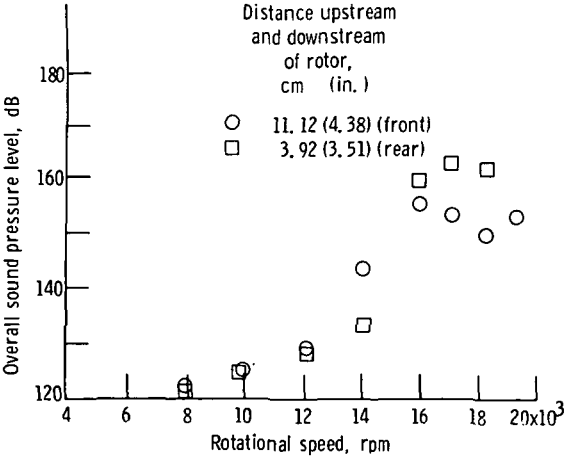

Figure 20. - Internal noise division, fore and aft of rotor with blade 1. Untwisted; rotor alone.

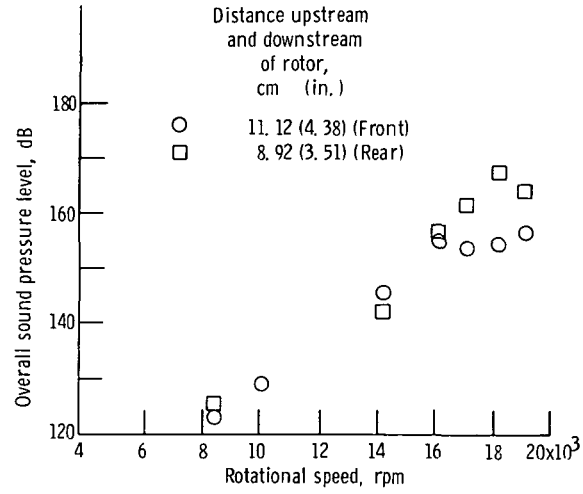

Figure 21. - Internal noise division fore and aft of rotor with blade 1. Twisted; rotor alone.

the rotor. This behaviour is good substantiation of the transfer of shock and expansion waves from front to back as the speed is increased. The rise in noise between 18 000 and 19 400 rpm for fan 1 does not fit the behaviour of the wave system models proposed here. The variation of amplitude with speed was also obtained in greater detail by tracking the blade passing tone as fan speed was varied, with tracking filter (fig. 22). Amplitude conversion from output voltage to decibels was accomplished by fitting the curves to the overall averages from the 32-second samples.

Comparison of the residual noise after establishment of the design wave configuration for rotors having twisted and untwisted blades shows (figs. 17 and 18) that the expected noise reduction was not achieved by twisting the blades and that the residual noise level of 154 decibels is higher than the predicted value of 149.2 decibels. These facts could both be explained by the presence of an additional source of noise that overwhelms

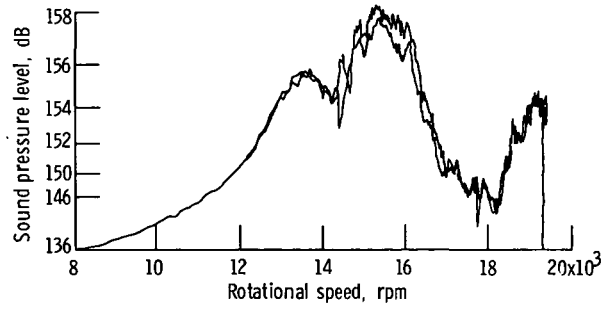

(a) Blade 1, twisted; distance upstream of rotor, 1.1 centimeters (0.42 in.).

Figure 22. - Blade passing tone noise of rotor; tracking of filter data.

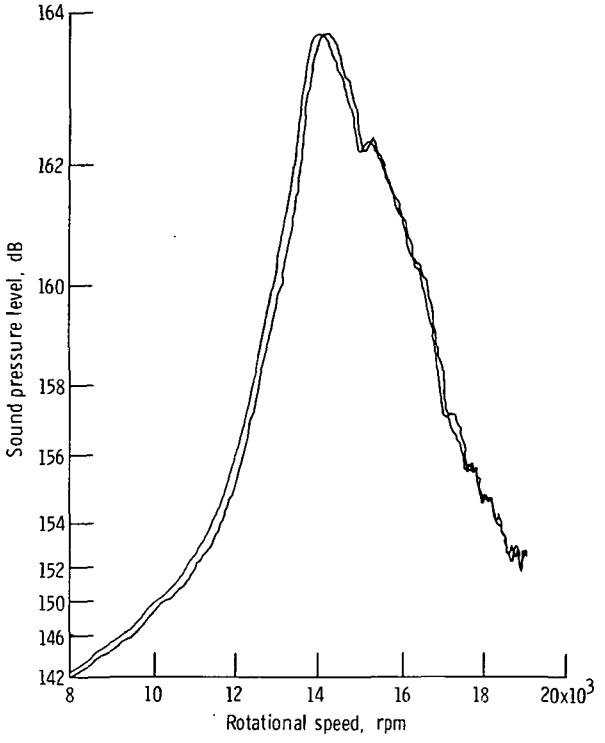

(b) Blade 2; distance upstream of rotor, 1.1 centimeters (0.42 in.).

Figure 22. - Concluded.

the effect of spanwise variation of the incidence angle and does not permit its reduction to be shown. (The predicted noise level was estimated from the previously calculated level of pressure fluctuation by assuming a linear variation of pressure fluctuation through zero along the span to account for the variation from compression to expansion wave. The rms values were then integrated spanwise for the sound level.)

The comparison of the noise levels shows that blades with profile 2 (fig. 19) with the flat suction surface, produced more noise at low supersonic speeds than blades with profile 1. Near design speed both types produce about the same noise. The straight-sided blade was expected to be less noisy because the wave configuration before starting (establishment of design configuration) did not have the upstream-propagating expansion wave originating on the suction surface. For the same reason the straight blade cannot have an attached shock wave propagating upstream and must therefore have the attached wave all propagating downstream. There can be no attached wave, then, unless the approach Mach number is sufficiently high for a 6° deflection. At low supersonic relative velocity, there is a large separation between the detached shock and the re-expansion waves, which originate on the blades. The propagation upstream may be expected to be better for the detached wave. As the Mach number increases, the shock

and re-expansion waves get closer, so that more rapid cancellation occurs, and sound transmission is reduced.

The level of noise gives some indication of the type of wave that produced it. A detached normal shock increases in strength with relative speed. The rotor with blade profile 2 (flat suction surface) could produce a detached shock wave (fig. 23) at 14 200 rpm (where the measured noise is greatest). The relative tip Mach number is then 1.045, and the normal shock pressure-rise ratio is 0.108. The corresponding saw-toothed wave has a fundamental noise level of 162 decibels and an overall value of

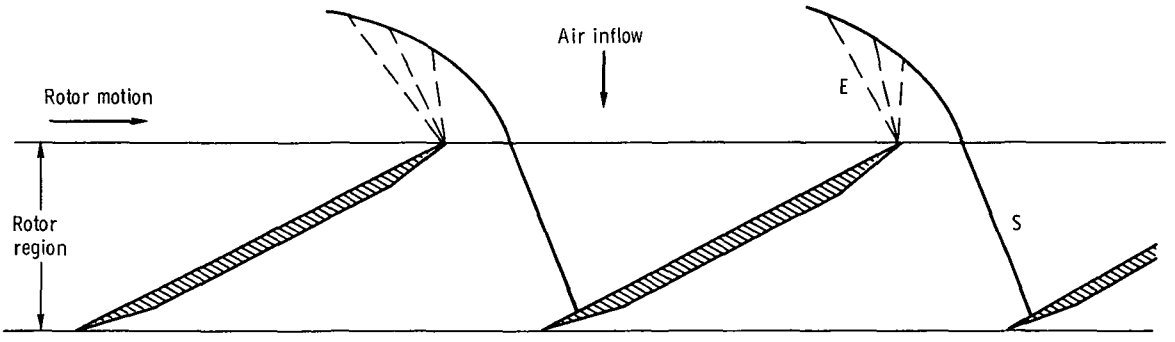

Figure 23. - Detached shock wave system at low supersonic speeds, blade 2. (S denotes shock waves; E expansion waves.)

164.2 decibels. If the expansion wave occupies two-thirds of the blade spacing, the wave-form is altered so that these levels are increased to 164 and 165.4 decibels, which agree well enough with measurements (fig. 22(b)) to indicate that the normal detached shock system probably exists for this rotor at this speed. The lowest speed at which an attached 6° deflection wave can be formed is at 17 250 rpm when the relative Mach number at the blade tips is 1.28. Here the shock pressure rise ratio has increased to 0.745 - a rise of 16.8 to 178.8 decibels for the fundamental of a saw-toothed wave. The measured value of 157.5 decibels at that speed is 21.3 decibels lower than the saw-toothed wave estimate; this discrepancy could be accounted for by assuming a wave width of about 2.8 percent of the blade spacing (1.52 mm or 0.060 in.). Such a thin wave system would weaken rapidly and also show a reduction in pressure amplitude at a small distance upstream of the rotor.

The general configuration is shown in figure 24 where there is a shock wave followed by a family of expansion waves for each blade. The remainder of the blade spacing has essentially no pressure variation until the next shock wave. The expansion wave fans out with increasing distance from the blade until it contacts the following shock.

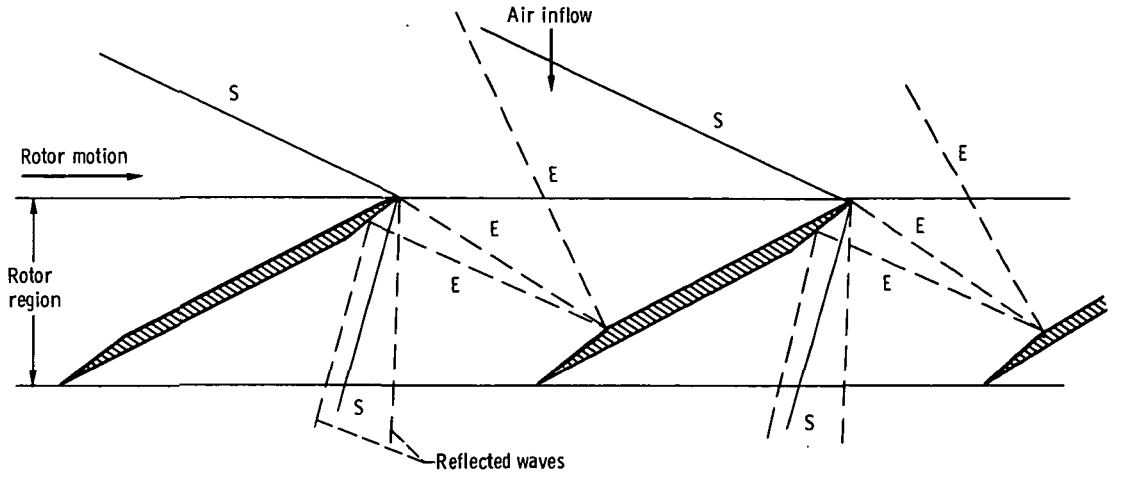

Figure 24. - Partially reflected wave system at low supersonic speeds, blade 1. (S denotes shock waves, E expansion waves.)

From this point on, the form of the wave is fixed as a saw-tooth, but the amplitude decreases with distance. In the region closer to the rotor, where there is no cascade interference effect, the wave form changes as the expansion region increases and the constant pressure region decreases. Attachment at the root could be accomplished at approximately 17 250×18/16 = 19 400 rpm, which is the highest speed tested; the tracking filter trace (fig. 22(b)) gives some indication that the sound pressure level has reached a minimum there of about 153 decibels. The detached wave has, for all practical purposes, been eliminated at the design speed.

As a check on the applicability of the model of the wave systems of blade profile 1, an estimate of the noise level is compared with measurement. After the wave becomes attached, it is reflected progressively with increasing speed (part speed, fig. 24; full speed, fig. 3). The forward-propagating wave system with 6° deflection is estimated at 15 300 rpm, which is the lowest speed for supersonic relative approach velocity. The calculation yields 167 decibels at station 1 as compared with a measurement of only 158 decibels (fig. 22(a)). As the speed is increased the measurements drop off to 148 decibels at 18 000 rpm and rise to 154 decibels at 19 400 rpm. All these measured values are much lower than would be expected for a 6° wave system, making it logical to conclude that these waves are diverted downstream by the following blades. The estimated speeds for this to occur are 19 200 rpm for the blade roots and 19 730 rpm for the blade tips. The low level produced by the fan, compared with the calculations from the postulated wave system indicates that the model is not quite adequate for the blade with the shaped suction (trailing) surface.

The residual blade passing noise level remaining after the design wave configuration

is achieved is about 153 to 154 decibels at 19 400 rpm. Two noise sources seem possible:

(1) Shock and expansion waves created by the bluntness of the leading edges (0.12 mm or 0.005 in.)

(2) Three-dimensional waves, which originate from the spanwise variation of the angle of incidence that makes it impossible to obtain zero incidence angle simultaneously on the entire span.

The leading-edge shock of a blunt wing has been described by Lighthill (ref. 5), and the possibility of its application to the problem of noise of supersonic fans by Fink (ref. 3).

An estimate of the noise based on this analysis was made for various rotative speeds as a function of axial location and plotted in figure 25. Details of the analysis

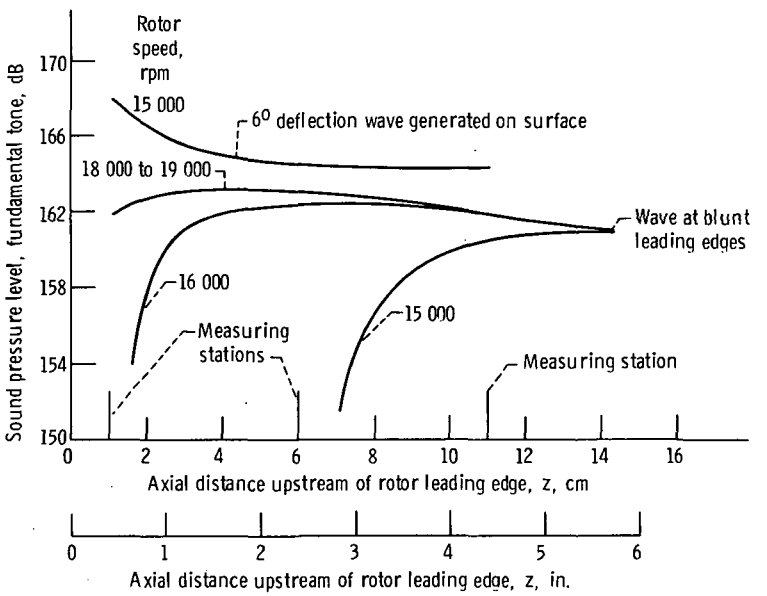

Figure 25. - Estimate of fundamental tone produced by shock-wave systems.

are given in appendix B. The high-speed value is of interest here because the amplitude of the other wave systems will have decreased to low levels and will be providing minimum interference. At 18 000 to 19 000 rpm the estimated sound pressure level of the fundamental tone at 1.1 centimeters upstream of the rotor and resulting from leading edge bluntness is 161.9 decibels. This is adequate to account for the magnitude of the observed residual sound. Also shown in figure 25 is the 6° deflection wave system generated on the surface for 15 000 rpm, which will be described in the next section.

TRANSMISSION OF ACOUSTIC WAVES

Because of differences in the transmission of various pressure disturbances in the fan inlet, the noise will vary in spectral content from one station to the next. Basically, the entire noise content at supersonic speeds is the blade passing tone; shaft harmonics are small for this fan.

Figures 17 to 19 display transmission when the noise levels at successive stations are compared. Subsonic data show severe damping as described by Tyler and Sofrin (ref. 13). This is not a dissipative phenomenon; the pressure fluctuations do not indicate acoustic energy because the velocity and pressure are out of phase. At supersonic velocities the shock waves formed have the pressure and velocity fluctuations in phase; therefore, vibrational energy is conducted. Variation along the annulus then results from nonlinear effects where expansion and shock waves cancel each other.

In the case of the detached shock wave resulting from a small amount of bluntness, there is an equal expansion wave originating from the leading edge just behind the shock. According to Lighthill (ref. 5), the pressure rise of the shock in this case varies inversely as the square root of the normal distance from the blade ($1/\sqrt{y}$) or distance upstream of the rotor face ($1/\sqrt{Z}$). At sufficiently large distances upstream, spreading the expansion waves results in a cascade effect where the shock wave then reacts as well with the expansion wave from the next leading blade. Then the shock pressure rise varies like $1/z$ (see Fink (ref. 3) and Morfey and Fisher (ref. 14)).

The wave system originating from the shaping of the suction surface and its accompanying shock follow a similar course, except that for this particular shape the shock wave initially interacts with the expansion wave from the preceding blade (fig. 24) and further upstream interacts with the following wave from the same blade. In both these wave systems, during the inital or one-side interaction phase the wave shape varies as a function of distance upstream of the rotor face because of the varying width of the expansion wave. The root-mean-square pressure fluctuation then is a varying fraction of the shock-wave pressure; it may increase as the shock strength decreases.

Calculations were made according to the models described and the results are plotted in figure 25. The noise levels calculated indicate that the sound pressure from the surface generated wave is dominant at 15 000 rpm, but at higher speed this noise reaches a low level, and the residual noise is produced by the blunt leading edges. Hence the sound at low supersonic speed should decrease about 3 decibels between the first two stations and be nearly constant to the third. At high speeds the level should rise about 1 decibel between the first two stations and then fall off about 1 decibel to the third. The data of blade 1 does not have these characteristic variations at low and high speeds nor the calculated noise levels. Reduction of the noise levels from that of the two-dimensional model must require a somewhat more complex model.

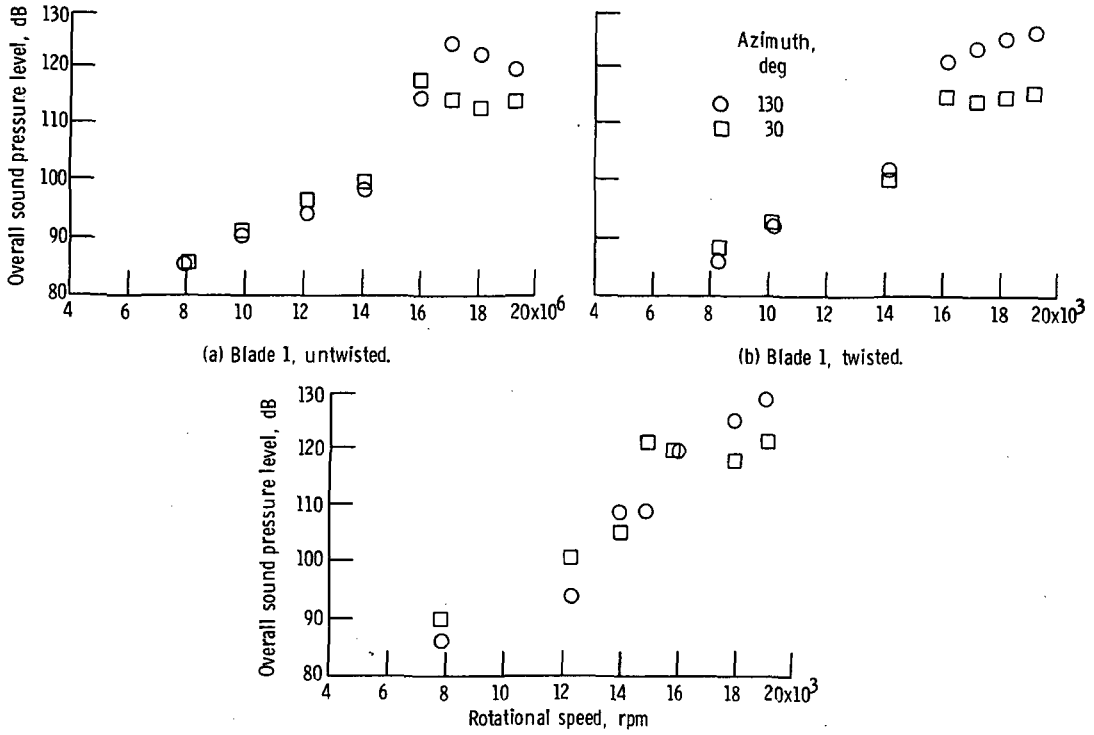

(a) Blade 1, untwisted.

(b) Blade 1, twisted.

(c) Blade 2.

Figure 26. - Far-field noise, rotor alone.

Far-field sound level as a function of speed is shown in figure 26. This shows the same trends with speed as the data measured in the annulus of the fan. Therefore, the swallowing of the frontal shock system, with a low residual noise level near design speed, produces an exterior noise level that reflects these changes. The noise level outside the fan can be reduced by the reduction of the internal wave system.

COMPLETE FAN STAGE

The introduction of the outlet guide vanes, which redirect the rotor discharge flow from a spiralling to an axially directed flow, will increase the noise level because of noise radiation from the stator vanes. These vanes intercept the rotor discharge wakes periodically, giving rise to interaction tones at the blade passing frequency. It is well known that these tones can be reduced to low levels by using large spacing between the blade rows.

When the stator assembly was inserted, the rear internal measuring station at 8.92 centimeters downstream of the rotor was immediately behind the stator blades. Noise was also measured at the station 11.1 centimeters upstream of the rotor. Over-

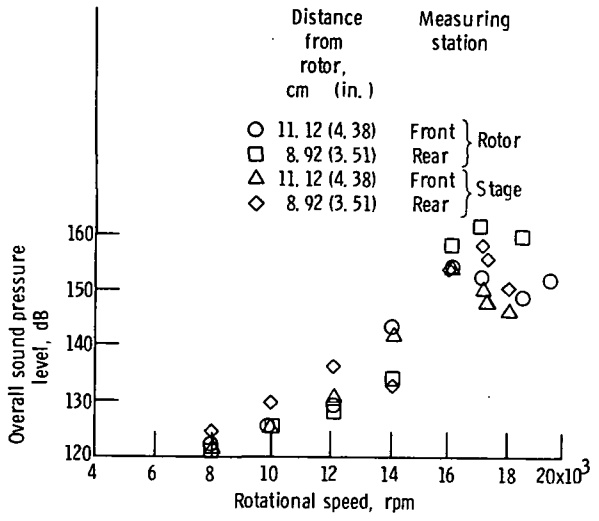

Figure 27. - Production of noise, comparison of rotor alone with complete stage; blade 1, untwisted.

all sound pressure level of the blade passing tone is displayed in figure 27 at those two stations with and without the outlet guide vanes. The front end noise is essentially unchanged by the presence of the outlet vanes, either at subsonic or supersonic speeds.

Radiation rearwards is increased by radiation from the vanes at subsonic speeds, but at supersonic speeds, the noise is decreased. The drop in sound pressure level at sonic speed (14 000 rpm), measured at the downstream internal station, to a level below that for 12 000 rpm indicates that the rotor blades wakes ceased to be an effective noise producer. At this and higher speeds, the blade passing tone is reduced by the presence of the vanes. The vanes evidently do not radiate additional noise caused by pressure fluctuations induced by shock wave impacts; rather they dissipate some of this sound energy.

CONCLUSIONS

Three rotors and a fan stage were tested with rotor blades that were designed to eliminate upstream progressing shock waves by the elimination of the corresponding expansion waves. These exhibited the following characteristics:

1. A large increase in noise with rotor speed as the relative gas velocity increased through sonic speed, indicating the inception of shock wave noise generation. With further speed increase the forward propagating noise decreased while the backward-propagating noise continued to increase and finally leveled off at a high intensity. This indicated the transfer of the pressure waves from the front of the rotor to the rear.

2. Blade shape 1, which generated forward-propagating waves at low supersonic speeds, produced less noise than blade shape 2 (flat suction surface). The expansion wave produced by the blade having a convex suction surface permitted the attachment of the bow wave at low supersonic velocity, thereby producing a weakening of the upstream wave system as the leading edges intercepted more of the expansion waves with increasing speed.

3. The residual blade passing tone at speeds near design could be caused by shock waves resulting from bluntness of the leading edges, but severe modification of this model is required to explain the reduced intensity measured and the difference of transmission from the theoretical prediction.

4. A supersonic fan with blading designed for low forward radiation of blade passing noise is feasible for a rotor with short blades.

5. The outlet guide vanes of the complete fan stage did not affect forward propagation of rotor noise.

6. The vanes radiated additional noise at subsonic speeds, but damped out rearward-propagating rotor noise at high speed.

7. Substantial variations in the pressure field from one blade passage to the next occurred at supersonic speeds.

Lewis Research Center,
National Aeronautics and Space Administration,
Cleveland, Ohio, September 8, 1972,
501-24.

APPENDIX A

SYMBOLS

A, B, C	shock wave constants (see appendix B)
a	angle of approach flow direction, to cascade axis direction
C_a	portion of blade chord under aerodynamic loading
F_θ	tangential component of blade force per unit height, exerted on gas
ΔH_T	rise in specific stagnation enthalpy of gas passing through fan
M	Mach number of flow
M_Z	Mach number of flow, axial component
P	free-stream pressure
ΔP	rise in stream pressure across shock
S	spacing of blades, measured in direction of rotation
ΔT_T	rise in stagnation temperature of gas passing through fan
U	rotational velocity of rotor blades
V_Z	axial component of gas velocity
y	distance normal to blade surface of a point on the leading-edge shock wave
Z	axial distance (parallel to axis of rotation)
α	pitch angle of blades
β	angle of characteristic line to upstream flow direction
γ	ratio of specific heats
ϵ	deflection angle of flow passing through shock wave
θ_w	shock wave angle to upstream flow vector
ξ	abbreviation symbol (see appendix B)
ρ	density of gas stream
σ	width of leading-edge wave system, measured parallel to cascade axis
τ	thickness of leading edge of airfoil

Subscripts:

0 upstream of shock

1 at axial location where the wave systems from adjacent blades mutually interfere ($\sigma = S$)

APPENDIX B

NOISE FROM BLUNT LEADING EDGES

For an isolated body with a blunt leading edge immersed in a supersonic stream, there is a detached shock followed by an expansion wave that causes the shock to weaken with distance and approach the direction of the free-stream characteristic.

Lighthill gives for the intensity of this wave, in terms of the pressure rise ratio $\Delta p/p_0$, the equation

$$\frac{\Delta p}{p_0} = 3\sqrt{\frac{\tau}{y}}$$

where Δp is the rise in static pressure through the shock wave, p_0 is the stream pressure upstream of the shock wave, τ is the leading-edge thickness, and y is the distance normal to the blade surface of a point on the shock wave (with $y > 10\tau$ (see fig. 28)). The wave angle of the shock wave is locally given by θ_w where

$$\tan \theta_w = \tan \beta_0 + A\theta + C\theta^2$$

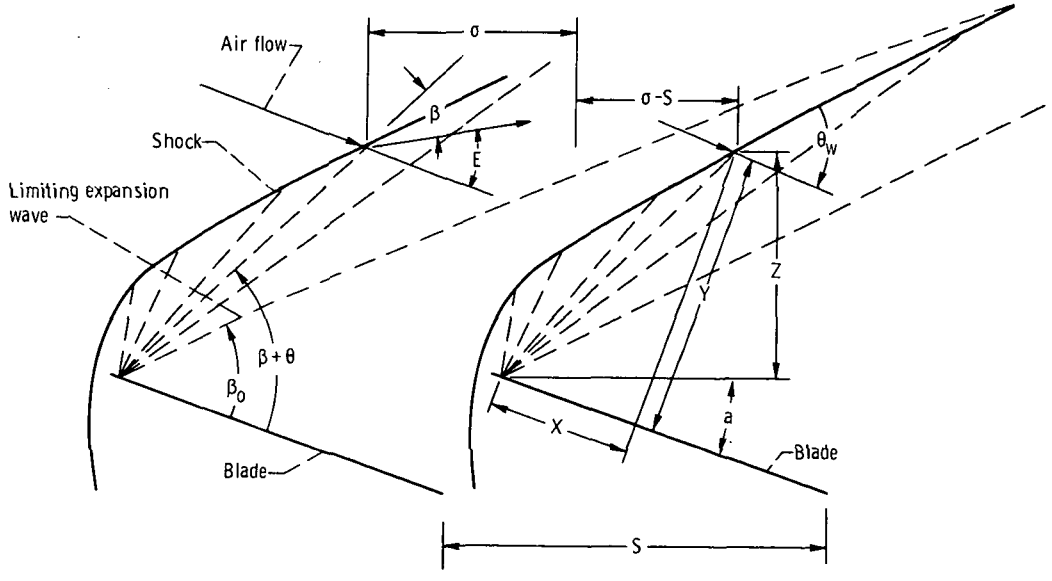

Figure 28. - Notation for shocks at blunt leading edges of cascade blades.

and the characteristic angle ($\beta = \sin^{-1}(1/M)$)

$$\tan(\beta + \epsilon) = \tan \beta_0 + 2A\theta + B\theta^2$$

where ϵ is the flow deflection angle and M_0 is the approach Mach number and where

$$\sin \beta_0 = \frac{1}{M_0}$$

$$A \equiv \frac{\gamma + 1}{4} \frac{M_0^4}{\left(M_0^2 - 1\right)^2}$$

$$B \equiv \frac{\gamma + 1}{2} \frac{M_0^4}{\left(M_0^2 - 1\right)^{7/2}} \left(1 + \gamma M_0^2\right)$$

$$C \equiv B \frac{(\gamma + 1)M_0^4 + 4(\gamma - 1)M_0^2 + 8}{16\left(1 + \gamma M_0^2\right)}$$

If one specifies $\Delta p/p$ and M_0, then the shock angle θ_w is

$$\sin \theta_w = \frac{1}{M_0} \sqrt{1 + \frac{\gamma + 1}{2\gamma} \frac{\Delta p}{p_0}}$$

and deflection is then

$$\tan \epsilon = \frac{\frac{\Delta p}{p_0}}{\left(\gamma M_0^2 - \frac{\Delta p}{p_0}\right) \tan \theta_w}$$

Then after the calculation of $\beta + \epsilon$, the cascade geometry is introduced (τ, a) and the

distance z of the point upstream of the cascade is given by

$$z = \tau \frac{9}{(\Delta p/p)^2} \frac{\sin(\beta + \epsilon - a)}{\sin(\beta + \epsilon)}$$

where τ is the thickness of the leadinge edge. The width σ of the expansion fan measured parallel to the cascade axis is

$$\sigma = z \frac{\sin(\beta + \epsilon - \beta_0)}{\sin(\beta + \epsilon - a) \sin(\beta_0 - a)}$$

This may be compared with the spacing s to determine whether the wave systems of the blades are interfering with each other and to estimate the form of the pressure wave as a function of time at any one location. This calculation may be carried out as far as $\sigma = s$; from this point on the interference must be accounted for. The variation of pressure with distance, in the case of mutual interference, follows the approximate law given by Fink (ref. 3) and by Morfey and Fisher (ref. 14). That is, for a saw-toothed wave

$$\frac{\Delta p}{p_0} = \frac{\left(\frac{\Delta p}{p}\right)_1}{1 + \frac{\gamma + 1}{2\gamma}\left(\frac{\Delta p}{p}\right)_1 \xi}$$

where $(\Delta p/p)_1$ is the pressure rise ratio at the location $z = z_1$,

$$\xi \equiv \frac{\frac{z - z_1}{s}}{\left[\cos(\beta_0 - a) - M_0 \sin a\right] \sin(\beta_0 - a)}$$

and where $\sigma = s$.

In the region where there is no interference ($z < z_1$), the wave form has a root mean square value of

$$\frac{p_{rms}}{p_0} = \frac{\Delta p}{p_0} \sqrt{\frac{\left(\frac{4 - 3\sigma}{s}\right)\frac{\sigma}{s}}{12}}$$

For $z > z_1$ the fixed-form saw-toothed wave then continues with $\sigma = s$ and $p_{rms} = \Delta p/\sqrt{12}$. It is noteworthy that in the region where σ/s is sufficiently small, the rms value p_{rms} can increase with distance from the rotor even though the wave amplitude may be decreasing like $1/\sqrt{z}$. The fundamental tone component of such a wave is

$$\frac{p_{rms}}{p_0} = \frac{\Delta p}{p_0} \frac{1}{\pi\sqrt{2}} \sqrt{\sin^2 \pi \frac{\sigma}{s} + \left(\frac{\sin \pi \frac{\sigma}{s}}{\pi \frac{\sigma}{s}} - \cos \pi \frac{\sigma}{s}\right)^2}$$

REFERENCES

1. Ferri, Antonio: The Supersonic Compressor. II - Aerodynamic Properties of Supersonic Compressors. Aerodynamics of Turbines and Compressors. W. R. Hawthorne, ed., Princeton Univ. Press, 1964, pp. 381-397.

2. Philpot, M. G.: The Buzz-Saw Noise Generated by a High Duty Transonic Compressor. Paper 70-GT-54, ASME, May 1970.

3. Fink, M. R.: Shock Wave Behaviour in Transonic Compressor Noise Generation. Paper 71-GT-7, ASME, 1971.

4. Goldstein, Arthur W.; Glaser, Frederick W.; and Coats, James W.: Acoustic Properties of a Supersonic Fan. Paper 71-182, AIAA, Jan. 1971.

5. Lighthill, M. J.: Higher Approximations. General Theory of High Speed Aerodynamics. William R. Sears, ed., Princeton Univ. Press, 1954.

6. Kester, J. D.; and Slaiby, T. G.: Designing the JT9D Engine to Meet Low Noise Requirements for Future Transports. Paper 670331, SAE, Apr. 1967.

7. Ehrich, F. F.: Acoustic Resonance and Multiple Pure Tone Noise in Turbomachinery Inlets. Paper 69-GT-2, ASME, Mar. 1969.

8. Mather, J. S. B.; Savidge, J.; and Fisher, M. J.: New Observations on Tone Generation in Fans. J. Sound Vib., vol. 16, no. 3, June 8, 1971, pp. 407-418.

9. Goldstein, Arthur W.; Lucas, James G.; and Balombin, Joseph R.: Acoustic and Aerodynamic Performance of a 6-Foot-Diameter Fan for Turbofan Engines. II - Performance of QF-1 Fan in Nacelle Without Acoustic Suppression. NASA TN D-6080, 1970.

10. Sofrin, T. G.; and Pickett, G. F.: Multiple Pure Tone Noise Generated by Fans at Supersonic Tip Speed. Presented at the International Symposium on Fluid Mechanics and Design of Turbomachinery, Pennysylvania State Univ., 1970.

11. Hawkings, D.: Multiple Tone Generation by Transonic Compressors. J. Sound Vib., vol. 17, no. 2, July 22, 1971, pp. 241-250.

12. Kurosaka, M.: A Note on Multiple Pure Tone Noise. J. Sound Vib., vol. 19, no. 4, Dec. 22, 1971, pp. 453-462.

13. Tyler, J. M.; and Sofrin, T. G.: Axial Flow Compressor Noise Studies. Trans. SAE, vol. 70, 1962, pp. 309-332.

14. Morfey, C. L.; and Fisher, M. J.: Shock-Wave Radiation From a Supersonic Ducted Rotor. Aeron. J., vol. 74, no. 715, July 1970, pp. 579-585.

"The aeronautical and space activities of the United States shall be conducted so as to contribute . . . to the expansion of human knowledge of phenomena in the atmosphere and space. The Administration shall provide for the widest practicable and appropriate dissemination of information concerning its activities and the results thereof."

—NATIONAL AERONAUTICS AND SPACE ACT OF 1958

NASA SCIENTIFIC AND TECHNICAL PUBLICATIONS

TECHNICAL REPORTS: Scientific and technical information considered important, complete, and a lasting contribution to existing knowledge.

TECHNICAL NOTES: Information less broad in scope but nevertheless of importance as a contribution to existing knowledge.

TECHNICAL MEMORANDUMS: Information receiving limited distribution because of preliminary data, security classification, or other reasons. Also includes conference proceedings with either limited or unlimited distribution.

CONTRACTOR REPORTS: Scientific and technical information generated under a NASA contract or grant and considered an important contribution to existing knowledge.

TECHNICAL TRANSLATIONS: Information published in a foreign language considered to merit NASA distribution in English.

SPECIAL PUBLICATIONS: Information derived from or of value to NASA activities. Publications include final reports of major projects, monographs, data compilations, handbooks, sourcebooks, and special bibliographies.

TECHNOLOGY UTILIZATION PUBLICATIONS: Information on technology used by NASA that may be of particular interest in commercial and other non-aerospace applications. Publications include Tech Briefs, Technology Utilization Reports and Technology Surveys.

Details on the availability of these publications may be obtained from:

SCIENTIFIC AND TECHNICAL INFORMATION OFFICE

NATIONAL AERONAUTICS AND SPACE ADMINISTRATION

Washington, D.C. 20546